Pediatr Radiol (2015) 45:5–19
DOI 10.1007/s00247-014-3067-0

MINISYMPOSIUM

Advances in cardiac magnetic resonance imaging of congenital heart disease

Mieke M. P. Driessen · Johannes M. P. J. Breur · Ricardo P. J. Budde · Joep W. M. van Oorschot · Roland R. J. van Kimmenade · Gertjan Tj Sieswerda · Folkert J. Meijboom · Tim Leiner

Received: 20 February 2014 / Accepted: 21 May 2014

Abstract Due to advances in cardiac surgery, survival of patients with congenital heart disease has increased considerably during the past decades. Many of these patients require repeated cardiovascular magnetic resonance imaging to assess cardiac anatomy and function. In the past decade, technological advances have enabled faster and more robust cardiovascular magnetic resonance with improved image quality and spatial as well as temporal resolution. This review aims to provide an overview of advances in cardiovascular magnetic resonance hardware and acquisition techniques relevant to both pediatric and adult patients with congenital heart disease and discusses the techniques used to assess function, anatomy, flow and tissue characterization.

Electronic supplementary material The online version of this article (doi:10.1007/s00247-014-3067-0) contains supplementary material, which is available to authorized users.

M. M. P. Driessen · R. P. J. Budde · J. W. M. van Oorschot · T. Leiner (✉)
Department of Radiology, University of Utrecht,
University Medical Center Utrecht,
PO Box 85500, 3508 GA Utrecht, The Netherlands
e-mail: t.leiner@umcutrecht.nl

M. M. P. Driessen · R. R. J. van Kimmenade · G. T. Sieswerda · F. J. Meijboom
Department of Cardiology, University of Utrecht,
University Medical Center Utrecht,
PO Box 85500, 3508 GA
Utrecht, The Netherlands

M. M. P. Driessen
The Interuniversity Cardiology Institute of the Netherlands (ICIN) – Netherlands Heart Institute, PO Box 19258, 3501 DG Utrecht,
The Netherlands

J. M. P. J. Breur · F. J. Meijboom
Department of Pediatric Cardiology, Wilhelmina Children's Hospital, University Medical Center Utrecht,
PO Box 85500, 3508 GA Utrecht, The Netherlands

Keywords Cardiovascular magnetic resonance · Technical advances · Congenital heart disease · Child · Magnetic resonance imaging

Introduction

Congenital heart defects are the most frequently encountered congenital disorders. [1] The incidence of congenital heart defects reported in literature varies between 4 and 50 cases per 1,000 live births depending on the definition used [2]. Natural survival to adulthood for moderate to severe congenital heart defects – i.e. conduits, transposition of the great arteries, Tetralogy of Fallot or univentricular hearts – is less than 50%. Due to advances in cardiac surgery, survival has increased considerably during the past decades and >96% of patients with congenital heart defects – surviving their first year – will be alive at 16 years of age [2, 3]. Despite these advances, residual lesions requiring reoperation and complications like ventricular dysfunction and arrhythmia are prevalent in this population and require follow-up over time. Another important group in pediatric cardiology are patients with ventricular dysfunction due to a cardiomyopathy – classified as dilated, restrictive, hypertrophic, arrythomogenic or unclassified cardiomyopathy – with a cumulative incidence of about 1.24 per 100,000 children younger than 10 years of age [4, 5]. The increasing number of childhood cancer survivors, estimated to be one in every 540 adults in the United States, adds to this group due to anthracycline-induced cardiotoxicity leading to left ventricular dysfunction and – in a subgroup – to dilated or restrictive cardiomyopathy [6].

In patients with congenital heart defects and cardiomyopathies, cardiac imaging is important to diagnose the presence and extent of cardiac and extracardiac pathology, to determine the optimal treatment strategy and to provide the referring physician with a detailed overview of pre-procedural intra- and extracardiac anatomy. Although echocardiography

remains the first-line imaging modality in pediatric patients, cardiac magnetic resonance (MR) imaging has become the most important subsequent imaging modality for follow-up of children with cardiac disease. The major advantages of cardiac magnetic resonance imaging over other imaging modalities such as cardiac catherization and CT are that cardiac magnetic resonance imaging is noninvasive, it avoids application of ionizing radiation and can provide physiological, functional and anatomical information, all within a single examination.

Challenges of cardiac magnetic resonance imaging in patients with congenital heart disease

Obtaining high-quality cardiac MR imaging examinations in children has inherent challenges. The anatomical structures that have to be visualized are smaller, heart rates are higher and the ability to perform long and repeated breath-holds is limited. This requires the cardiac MR imaging acquisitions to be of both higher spatial and temporal resolution than in adults, with short imaging times and preferably without sequential breath-holds. As spatial resolution, acquisition time and signal-to-noise ratio are inherently dependent on each other, higher spatial resolutions and shorter imaging times will lead to decreased signal-to-noise ratio (Fig. 1). Fortunately, advances in cardiac MR imaging hardware, acquisition techniques and image reconstruction have mitigated this trade-off enabling high-quality imaging at short acquisition times. This review aims to provide an overview of the advances in cardiac MR imaging hardware and acquisition techniques that are important for imaging pediatric and adult patients with congenital heart disease and discusses relevant advances in cardiac MR imaging techniques used to assess function, anatomy, flow and tissue characterization (Table 1).

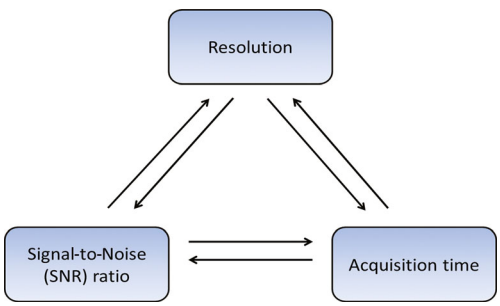

Fig. 1 MR imaging constraints. With MR imaging there is an inherent trade-off in each imaging protocol between spatial and temporal resolution, acquisition time and signal-to-noise ratio. For example, increasing spatial and temporal resolution will always lead to decreased signal-to-noise ratio or longer acquisition times when all other sequence parameters are kept equal. Improving one factor will therefore always negatively influence the other unless additional adaptations are made

Table 1 Summary of new sequences in cardiac magnetic resonance imaging

CMR indication	New sequences
General techniques	Respiratory navigator-gating
	Real-time imaging
Function	3-D-balanced SSFP
	Myocardial perfusion imaging
Anatomy	Single-shot BB
	Non-contrast-enhanced MRA
	4-D (time-resolved) MRA
Flow	4-D phase-contrast imaging
	3-D late gadolinium enhancement (PSIR)
	BB-STIR (edema)
Tissue characterization	T1 mapping

3D 3-dimensional, *SSFP* steady-state free precession, *BB* black blood, *4D* 4- dimensional, *MRA* magnetic resonance angiography, *PSIR* phase-sensitive inversion recovery, *STIR* short-T1 inversion recovery

Technical advances

Hardware

The most obvious change in MR hardware has been the introduction of higher field strengths greater than 1.5 T. Many facilities worldwide have installed 3-T field-strength magnets for use in cardiovascular imaging as all major vendors now offer large field-of-view capabilities with advanced transmit and receive coil arrays. Imaging at 3 T has the advantage of an intrinsically higher signal-to-noise ratio, which ameliorates the trade-off between higher spatial resolution, faster acquisitions and high signal-to-noise ratio [7]. However, imaging at higher field strengths is also associated with increased image artifacts due to inhomogeneties in the main magnetic field (B_0) and nonuniform radiofrequency excitation (B_1). Advanced radiofrequency shimming algorithms as well as adiabatic excitations have been developed to address these problems [8].

Parallel to the introduction of high field imaging, several other developments in MR hardware have greatly impacted cardiac magnetic resonance imaging in the past decades. Improved gradient performance has enabled much shorter repetition times (TR) and image acquisition duration [9, 10]. Further improvements in gradient performance, however, are limited by physiological and safety constraints such as radiofrequency-induced heating and peripheral nerve stimulation [11, 12].

The introduction of multi-array, highly sensitive receiver coils is another strategy that enables accelerated acquisition, while maintaining adequate signal-to-noise ratio, by using parallel imaging techniques. With parallel imaging, a reduced dataset in the phase encoding directions of k-space is acquired by using multiple coils elements simultaneously for signal

reception [13, 14]. Sensitivity encoding (SENSE) and generalized autocalibrating partially parallel acquisition are the parallel imaging techniques most frequently used. These techniques are, however, fundamentally different. Generalized autocalibrating partially parallel acquisition acquires reduced data in the frequency domain – before Fourier transformation – and sensitivity encoding in the imaging domain – i.e. after Fourier transformation. The factor by which acquisition duration is reduced is roughly equal to the parallel imaging factor, depending on which parallel imaging algorithm is used. Because undersampling is inherent in parallel imaging strategies it is important to obtain a sensitivity profile of each coil element in reference to a sensitivity map of the body coil, to avoid reconstruction artifacts. In the generalized autocalibrating partially parallel acquisition algorithm, this calibration step is integrated into the acquisition by acquiring several additional k-space lines, whereas in the sensitivity encoding algorithm the calibration is performed in a separate reference acquisition.

A final advance in MR hardware has been the introduction of small microchips that enable conversion of the analog signal picked up by the receiver coil to a digital signal in the receiver coil itself. The major advantage of this technology is the preservation of signal-to-noise, which is otherwise reduced by having to travel through receiver cables [15].

Undersampled acquisition

At present, image acceleration due to advances in hardware is limited to approximately a factor of about 10, but advances in pulse sequence design have enabled further gains in imaging speed [16]. Undersampling is the most frequently applied strategy; the basic principle is that k-space is undersampled using different sampling strategies or data sharing – also called view-sharing – exploiting spatial redundancy, temporal redundancy or both. By acquiring only part of the k-space the acquisition is accelerated. Variable-density techniques are commonly used for undersampling k space. The most often used strategy is sampling the center more frequently than the peripheral k-space. As only part of k-space is filled, missing data have to be reconstructed using specific, optimized algorithms to obtain accurate and artifact-free images. Some of the most frequently used strategies include keyhole-4-D TRAK, BRISK, CURE, TRICKS, TWIST and others (Table 2). For a detailed description of these techniques, we refer to the excellent overview by Tsao and Kozerke [16].

A recently introduced method for k-space undersampling known as compressed sensing deserves specific mention. In compressed sensing, k-space is sampled in a near-random fashion, which results in aliasing artifacts presenting as noise rather than discrete "image-like" foldover artifacts. In compressed sensing, iterative reconstruction techniques and various a priori constraints are used to suppress the noise due to aliasing, thus enabling faster and/or higher-resolution MR imaging [17]. In various studies, investigators have demonstrated the synergistic benefits of parallel imaging in combination with compressed sensing in children [18, 19].

Motion compensation

Of particular interest in pediatric patients are techniques to compensate for patient motion. With regard to cardiac imaging, three types of motion can be distinguished: 1) cardiac motion, 2) respiratory motion and 3) bulk motion (e.g., due to the inability of the subject to lie still in one position).

For cardiac imaging, motion-free periods suitable for anatomical imaging are end systole (rest period of approximately 50 ms) or mid-diastole (variable rest period, mainly dependent on heart rate). Advanced MR imaging platforms have the ability to target both of these rest periods selectively for imaging. Note that acquisition duration can be calibrated carefully to the exact rest period duration by varying the number of k-space lines acquired (in increments of 1 TR or several ms). Thus, in contrast to CT imaging where the heart rate often needs to be adapted to the rotation time of the CT scanner by using beta blockers, MR imaging specifically allows for tailoring the acquisition to the patients' heart rate.

The easiest way to compensate for respiratory motion is breath-holding performed by the patient. In cases where this is not possible, monitoring diaphragmatic motion with dedicated sequences offers a reliable alternative strategy, albeit at the expense of scanning efficiency [20]. Recently, several groups have proposed the idea of self-navigation, an approach whereby information about respiratory motion-induced displacement of the heart is obtained by oversampling the center of k-space relative to the peripheral part [21–23]. The main advantage of self-navigation schemes is the much better scan efficiency (up to 100% vs. approximately half this value for conventional respiratory navigator gating). The same principles employed for cardiac and respiratory motion compensation can be applied to correct for bulk motion as well. For detailed information about these techniques, the reader is referred to the excellent review of motion compensation strategies in MRI by van Heeswijk et al. [24].

Anatomy

Black-blood imaging

High-contrast black-blood images are very well suited for morphological assessment of cardiac structures. In many institutions, black-blood imaging with a standard (double inversion recovery) spin-echo pulse sequence is part of the routine imaging protocols. However, conventional black-blood imaging uses single-slice breath-holds, which is time-consuming and less favorable in children. To overcome this, various single-shot

Table 2 Cardiac magnetic resonance imaging acquisition techniques: vendor cardiovascular MR acronyms

Technique	Philips	Siemens	GE	Toshiba	Hitachi
(Turbo/Fast) spin echo	TSE	TSE	FSE	FSE	FSE
Single-shot T/FSE	Single-shot TSE	HASTE	Single-shot FSE	FASE	Single-shot FSE
Balanced SSFP	Balanced FFE	True FISP	FIESTA	True SSFP	Balanced SARG
Spoiled gradient echo	T1-FFE	FLASH	SPGR	FastFE	RF spoiled SARGE
Ultrafast gradient echo	TFE	TurboFLASH	Fast GRE/SPGR	Fast FE	RGE
(Turbo) gradient spin echo	GRASE	Turbo GSE,TGSE	-	Hybrid EPI	-
Dynamic MRA with k-space manipulation	Keyhole (4D-TRAK)	TWIST	TRICKS-XV	Freeze Frame	TRAQ
Parallel imaging:					
Frequency domain		GRAPPA			
Image domain	SENSE	mSENSE	ASSET	SPEEDER	RAPID
Multichannel RF coil sensitivity normalization	CLEAR	Prescan Normalize	PURE		NATURAL
Undersampling techniques:					
Radial regime	Multi-vane	BLADE	PROPELLER	JET	RADAR
Half Fourier	Half scan	Half Fourier	½ NEX	AFI	Half scan
Central k-space filling	CENTRA	Elliptical Scanning	Elliptic Centric	DRKS	PEAKS
Respiratory movement:					
Respiratory gating	Trigger	Respiratory gated	Respiratory Comp	Respiratory gated	MAR
Phase encode recording to reduce motion	PEAR	PACE	RSPE		PERRM

TSE turbo spin echo, *FSE* fast spin echo, *HASTE* half Fourier acquisition single shot turbo spin echo, *FASE* acquisition double echo, *FFE* fast field echo, *TrueFISP* true fast imaging echo with steady state precession, *FIESTA* fast imaging employing steady state acquisition sequence, *SSFP* steady state free precession, *SARGE* spoiled steady state acquisition rewindedgradient echo, *FLASH* fast low angle shot, *SPGR* spoiled gradient echo recalled, *GRE* gradient recalled echo, *FE* fast echo, *SARGE* spoiled steady state acquisition rewinded gradient echo, *RGE* rewinded gradient echo, *GRASE* gradient and spin echo, *TGSE* turbo gradient spin echo, *EPI* echo planar imaging, *4D-TRAK* 4-dimensional time-resolved angiography using keyhole, *TWIST* time-resolved angiography with stochastic trajectories, *TRICKS* time-resolved imaging of constrast kinetics, *RF* radio frequency, *(m)SENSE* (modified) sensitivity encoding, *CLEAR* constant level appearance, *GRAPPA* generalized autocalibrating partial parallel acquisition, *ASSET* array spatial sensitivity encoding technique, *PURE* phased array uniformity enhancement, *RAPID* rapid acquisition through parallel imaging design, *CENTRA* contrast enhanced timing robust angiography, *PROPELLER* periodically rotated overlapping parallel lines with enhanced reconstruction, *NEX* number of excitations, *DRKS* differential rate k-space sampling, *RADAR* radial acquisition regime, *PEAKS* peak arterial enhancing K-space sequence, *PEAR* phase encoded artifact reduction, *PACE* prospective acquisition correction, *RSPE* respiratory-sorted phase encoding, *PERRM* phase encode reordering to reduce motion

techniques, either turbo or fast spin-echo using halfscan (undersampling) with sensitivity encoding or stimulated echo acquisition mode, have been developed and validated against conventional single breath-hold black-blood techniques [25, 26]. The single-shot black-blood techniques have imaging times as short as 180 ms, enabling respiratory navigator gating or single breath-hold multislice black-blood acquisitions, while maintaining high spatial resolutions (Fig. 2) [25].

Contrast-enhanced MR angiography

Three-dimensional contrast-enhanced MR angiography (MRA) can be considered the state-of-the-art technique for noninvasive assessment of the vasculature. The first report on feasibility of contrast-enhanced MRA in infant-like conditions was by Hernandez et al. [27] in 2001, who simulated infant imaging conditions in small baboons. Multiphase 3-D dynamic MRA was performed using a spoiled gradient recalled-echo sequence during quiet breathing, achieving excellent image quality for the great vessels [27]. However, the imaging times were still long (average of 23 s per phase) and the respiratory movement caused blurring of the images. Shorter acquisition times were achieved using the above discussed view-sharing techniques in combination with various interpolation techniques (i.e. keyhole-4-D TRAK, TWIST and TRICKS), which are very well suited for contrast-enhanced imaging. This permitted higher resolutions and time resolved – but high spatial resolution – 4-D MRA (Table 1), with almost equal signal-to-noise ratio, contrast-to-noise ratio and vessel sharpness for the great vessels as conventional single-phase 3-D MRA (Figs. 3 and 4) [28]. The main advantages over conventional 3-D MRA are that time-resolved MRA resolves the problem of contrast timing and adds diagnostic information such as visualization of intra- and extracardiac shunts in approximately 60% of the patients [28–30]. However, some smaller vascular structures might be depicted more clearly with conventional 3-D single-phase MRA [30]. Therefore, both techniques are often used in clinical practice to supplement each other. As breath-hold times limit the spatial resolution that can be obtained for MRA, and motion – either cardiac or

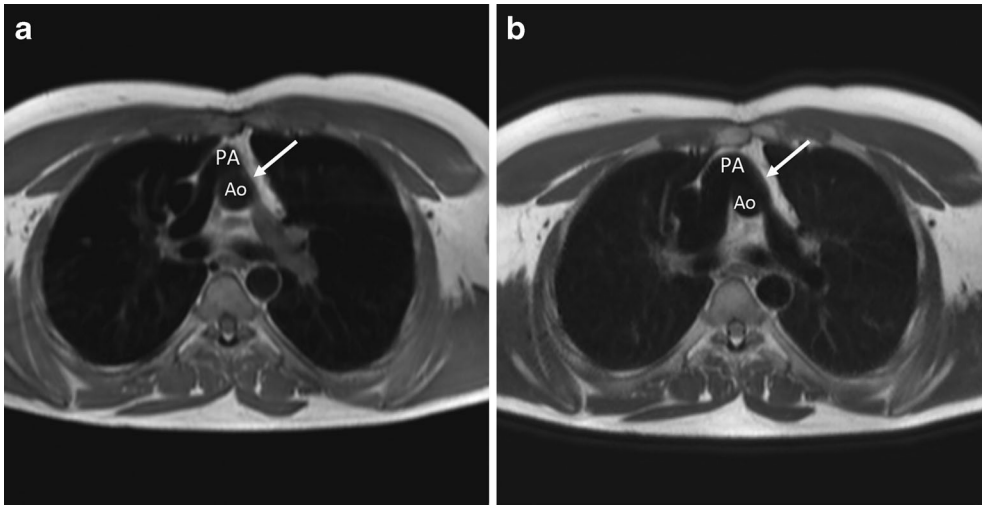

Fig. 2 Black-blood imaging. Black-blood images at the level of the pulmonary bifurcation of a 22-year-old man after arterial switch operation for transposition of the great arteries. Multiple breath-hold (**a**) and single-shot (**b**) black-blood images obtained at the level of the ascending aorta both depict a stenosis of the left branch of the pulmonary artery. Multiple breath-hold (**a**) used a multishot turbo spin-echo sequence with scan parameters: TR/TE: 857/10 ms, flip angle 90°, matrix 212×132, acquired voxel size 1.51×2.52 mm, slice thickness 8 mm, 18 slices and an acquisition duration of 120 s. For the single-shot black-blood image, a single-shot turbo spin-echo sequence was used with the following parameters: TE/TR: 857/50 ms, flip angle 90°, matrix 228×176, acquired voxel size 1.4×1.81 mm, slice thickness 8 mm, 12 slices and an acquisition duration of 11.4 s

respiratory – causes blurring of the MRA images, cardiac and respiratory-gated MRA was developed as described above. In patients with congenital heart disease, ECG- and respiratory-gated high-resolution MRA resulted in significantly improved delineation of (intra) cardiac anatomical structures and image quality, and vessel sharpness was equal to first-pass MRA [18, 30, 31]. However, to achieve high contrast-to-noise ratio during these relatively long acquisitions, two out of three studies used a blood pool contrast agent and the third study – Dabir et al. [31] – used a higher field strength [18, 31, 32].

Non-contrast-enhanced MRA

Volume-targeted or 3-D whole-heart non-contrast-enhanced (NCE) MRA techniques are well-suited to evaluate coronary anatomy and obstruction [33, 34] or to evaluate the thoracic vasculature in infants and pediatric patients (Figs. 4 and 5). Free-breathing 3-D radial steady-state free precession (SSFP) using respiratory movement correction is currently the method of choice to perform NCE-MRA [22, 33, 35]. To achieve maximum image contrast, a T2-preperation pulse and frequency-selective fat-suppression pulse are used. Recently, Bornert et al. [36] evaluated dual-echo Dixon fat suppression, which further improved image quality by delivering higher image contrast and diminishing ghosting and motion blurring. For optimal image quality, precise cardiac and respiratory gating (±2 mm) tailored to the individual patient is important. This can be hindered by heart rate variability, which decreases image quality and is especially a problem in children [37]. Generally, the imaging window is set to mid-diastolic resting period of the heart, in children – with high heart rates – this period is very short, resulting in motion blurring of the images. To avoid this, individual adaptations of the image window should be considered, in children and infants the end systolic resting period might provide better image quality than the mid-diastolic resting period (Fig. 5).

Function

B-SSFP cine imaging

Assessment of cardiac function using balanced SSFP (b-SSFP) cine imaging is one of the cornerstones of cardiovascular MR. Conventionally, single breath-hold multislice b-SSFP cine images are acquired in short-axis or axial orientation to cover the entire heart (online supplementary video), which is time-consuming and cumbersome. Starting the arrival of different acceleration techniques, single or dual breath-hold 4-D b-SSFP cine sequences have been developed using either highly parallel imaging, sensitivity encoding undersampling or compressed sensing (Fig. 6) [38–40]. Unfortunately, 3-D b-SSFP suffers from decreased blood-myocardial contrast and endocardial blurring, leading to underestimation of left and right ventricular volumes compared to conventional multislice techniques. To solve this, the use of intravascular contrast agents for 4-D b-SSFP was introduced, increasing image quality, blood-myocardial contrast and accuracy of volumetric measurements [39, 41]. In small children, the temporal and spatial resolution that can be achieved using 4-D b-SSFP might not be sufficient. To prevent multiple breath-holds in these patients, free-breathing respiratory gated multislice cine b-SSFP – using short

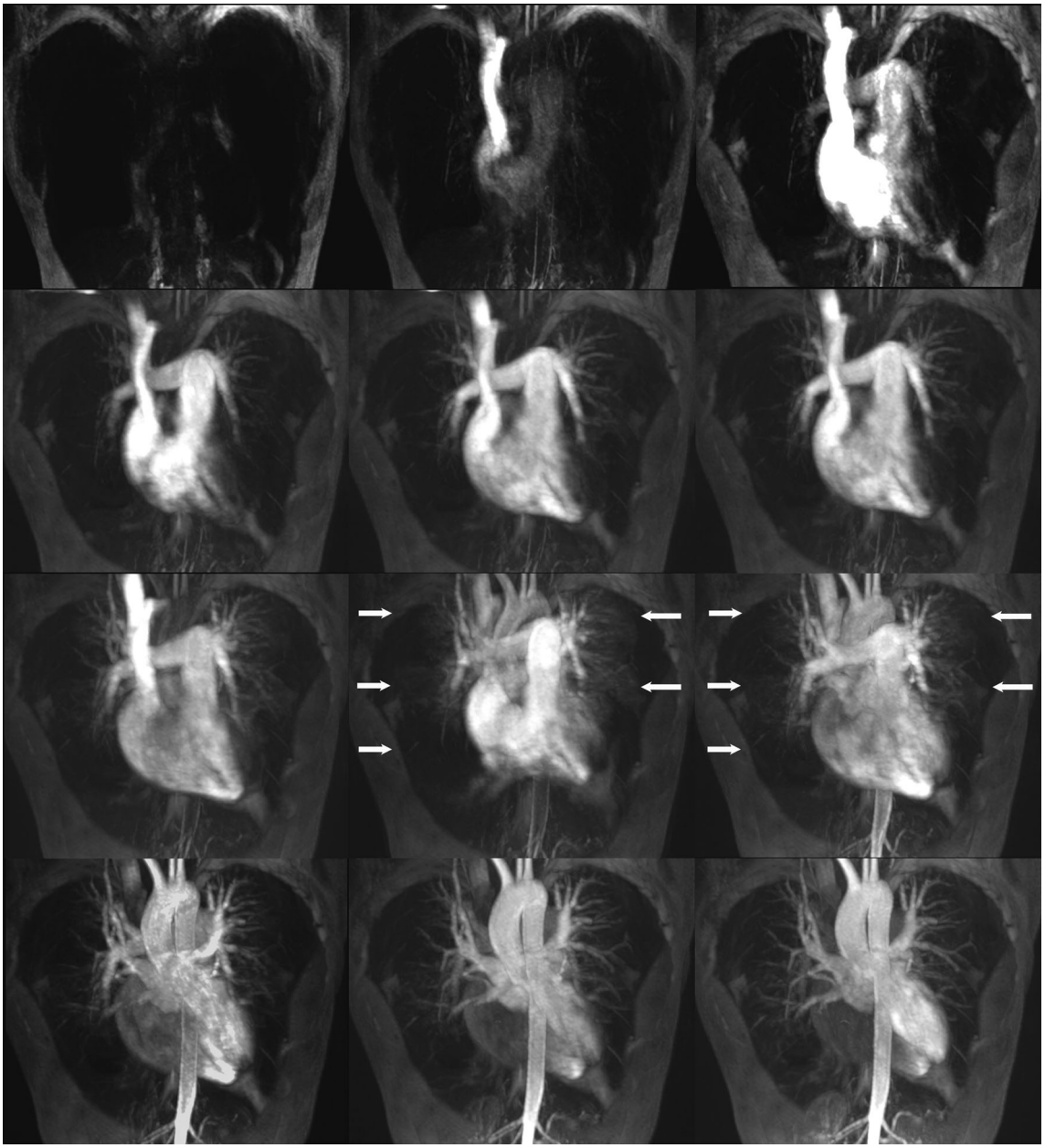

Fig. 3 Four-dimensional MRA of a 21-year-old women with chronic thrombo-embolic pulmonary hypertension shows successive full volume maximum intensity projections of a time-resolved gadolinium-enhanced MRA acquisition using a non-ECG-triggered spoiled gradient-echo sequence with SENSE (TR/TE 3.1/1.14 ms, flip angle 30°, matrix 268×267, acquired voxel size 1.49×1.49×4.6 slices, 60 slices, 12 dynamics, 3.4 s/per dynamic). There is clearly less pulmonary vascular enhancement in the right lung compared to the left lung (*arrows*)

echo and repetition time with multiple signal averages – can be used, which proved equally accurate as multislice acquisition for volumetric measurements [42].

Myocardial perfusion cardiovascular magnetic resonance

In adult cardiology, ischemia detection for coronary artery disease is one of the most important diagnostic questions. Myocardial perfusion MR imaging, using first-pass contrast enhancement of the myocardium during stress (with adenosine) and rest, has an excellent sensitivity and specificity to detect coronary artery stenosis (Fig. 7) [43–45]. Directly following contrast, infusion images are acquired dynamically using either gradient echo, SSFP with preperation (inversion or saturation) or hybrid echo-planar imaging (EPI)-gradient echo with preparation pulse. Undersampling and parallel imaging have improved ventricular coverage and imaging times; however, specificity at 1.5 T is still hampered by low signal-to-noise ratio, contrast-to-noise ratio and dark-rim artifacts [43, 46]. To improve myocardial perfusion

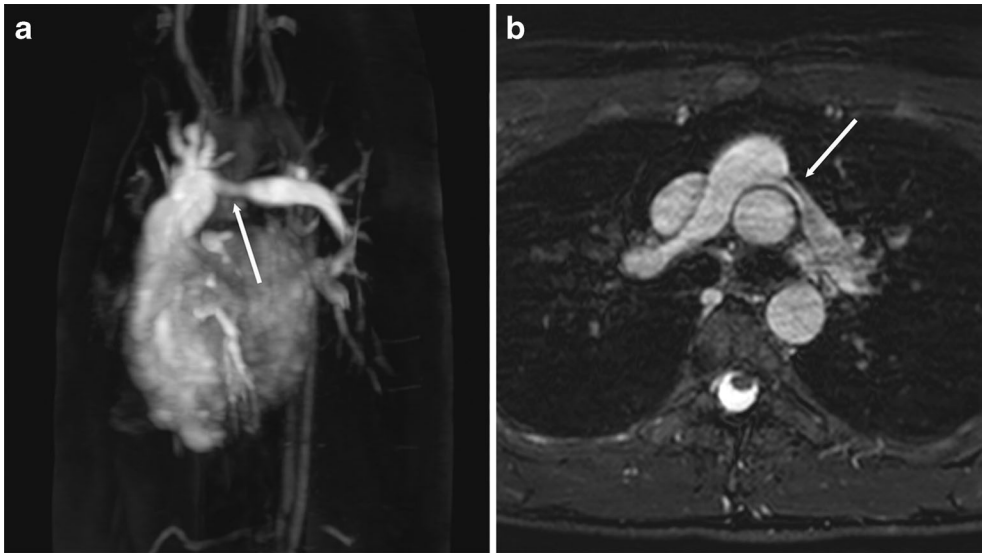

Fig. 4 Gadolinium-enhanced vs. non-contrast-enhanced MRA of a 16-year-old boy after arterial switch operation with a moderately severe left pulmonary artery stenosis. **a** Left anterior oblique maximum intensity projection of a dynamic gadolinium-enhanced MRA using a non-ECG triggered spoiled gradient-echo sequence (TR/TE 5.2/1.49 ms, flip angle 12°, matrix 192×171, acquired voxel size 0.94 × 0.94 × 2 mm, 60 slices, 2.8 s/per dynamic). **b** Corresponding non-contrast-enhanced respiratory navigator-gated balanced steady-state free precession MRA (TR/TE 4.9/2.4 ms, flip angle 90°, matrix 280×176, acquired voxel size 1.25×1.25×1.50 mm and 75 slices). Trigger delay was set to the end-diastolic resting period in this patient and acquisition duration at 80 ms per cardiac cycle

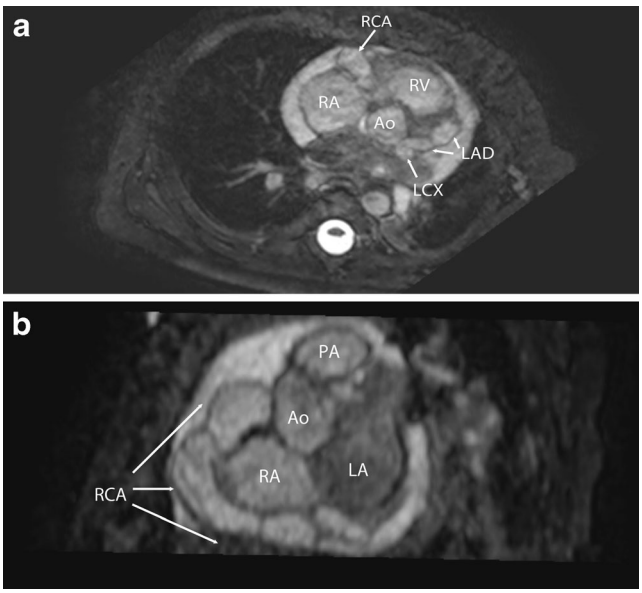

Fig. 5 Three-dimensional whole-heart non-contrast-enhanced (NCE) MRA in a 6-month-old boy with Kawasaki disease and grossly aneurysmatic coronary arteries. **a** Transverse source image at the level of the aortic root and left main coronary artery shows dilated right, left main, proximal left anterior descending and left circumflex coronary arteries (*arrows*). **b** Double oblique multiplanar reformation in left oblique sagittal orientation shows grossly dilated RCA. Note that the proximal right coronary artery has a diameter nearly equal to the aortic root (*arrows*; TR/TE 4.9/2.4 ms, flip angle 90°, TFE factor 16, matrix 280×176, acquired voxel size 1.25×1.25×1.50 mm and 75 slices). Because of the high heart rate the trigger delay was set to the endsystolic resting period. The acquisition duration was set to 50 ms per cardiac cycle

cardiovascular MR, higher field strengths (3 T) might be beneficial, as they improve signal-to-noise ratio and contrast-to-noise ratio and decrease dark-rim artifacts, improving diagnostic accuracy [44, 46]. Indications to perform myocardial perfusion investigations are less widespread in the pediatric population; however, it is of supplementary value in selected patient groups (i.e. aberrant coronary arteries or after reimplantation of the coronary arteries). The few studies performed in children demonstrate that myocardial perfusion imaging is feasible in this patient group and reported no serious adverse events related to adenosine infusion [47, 48].

Flow

Flow-sensitive imaging techniques allow for quantification of flow over time and are therefore useful in quantification of valve insufficiencies or shunt fractions (Qp:Qs) [49, 50]. Most frequently, a velocity-encoded, phase-contrast sequence is used, which is based on the principle that the phase of flowing relative to stationary spins along a magnetic gradient is proportionate to flow velocity. Velocity encoding can determine through-plane flow using phase-encoding or in-plane velocity, using frequency encoding. In case of valvular stenosis, both techniques might be used to obtain the best assessment possible. A major disadvantage of 2-D flow measurements is the inability to take into account the valve displacement during the cardiac cycle; direct measurements will likely underestimate the true regurgitate volumes of atrioventricular valves [51]. Furthermore, flow is

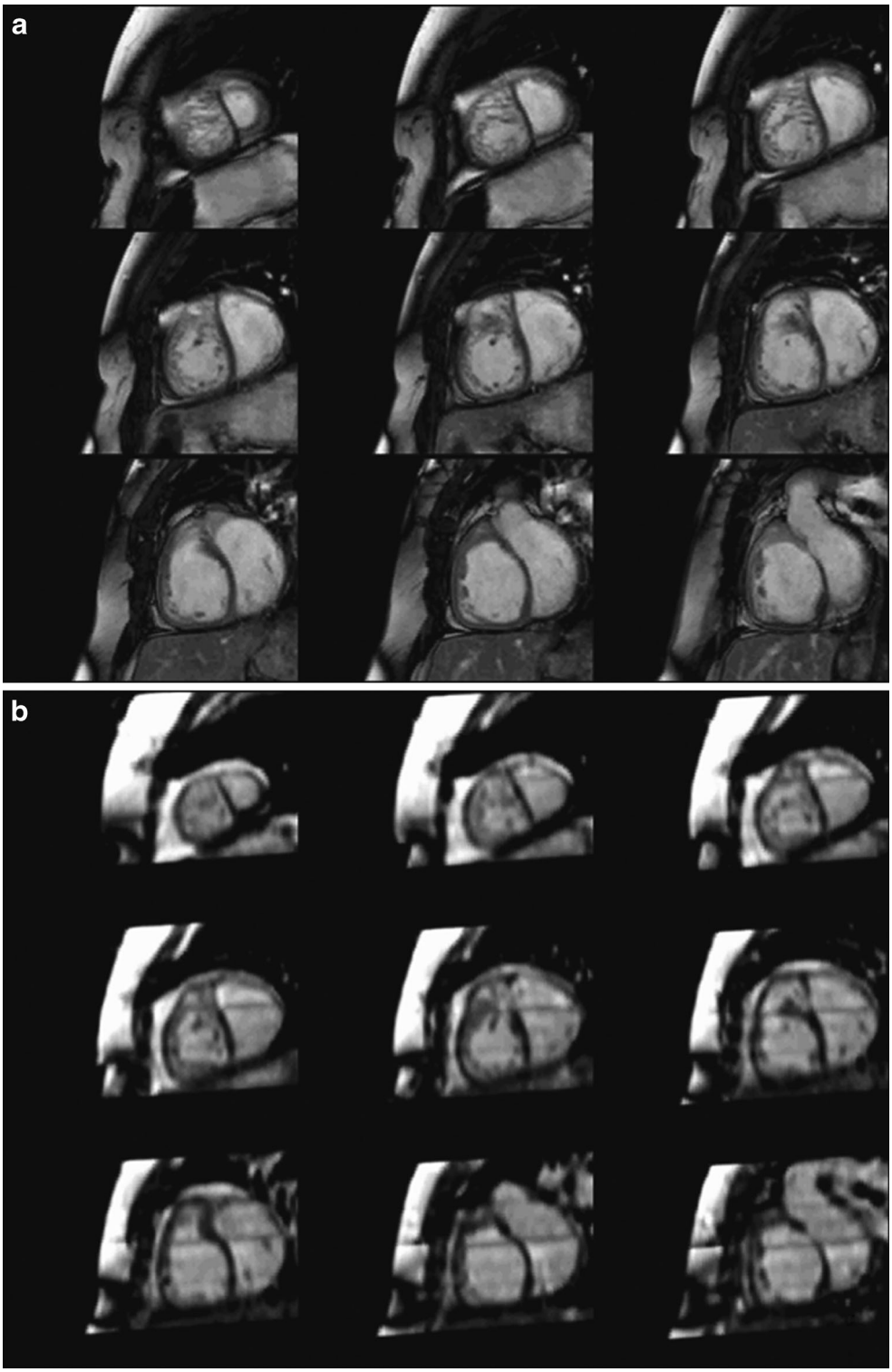

Fig. 6 Dual breath-hold whole-heart cine. Conventional single breath-hold per slice 2-D cine images (**a**) and reconstructed dual breath-hold 3-D whole-heart cine images (**b**) in the short-axis orientation, obtained in a 24-year-old man with repaired Tetralogy of Fallot. Three-dimensional whole-heart cine images (**b**) can be retrospectively reconstructed in every desired imaging plane. However, due to the isotropic acquisition with much thinner slices compared to conventional cine imaging, there is lower in-plane spatial resolution and lower blood-to-myocardium contrast. Conventional cine images were acquired with a balanced steady-state free precession sequence (**a**), scan parameters: TE/TR 1.7/3.4 ms, flip angle 60°, matrix 192×183, voxel size 1.25×1.25 mm, slice thickness 8 mm, 30 cardiac phases. For the dual breath-hold whole-heart cine images (**b**), a balanced steady-state free precession sequence was employed with the following scan parameters: TE/TR 1.4/2.8 ms, flip angle 50°, matrix 144x144x25, voxel size 2.43×2.43×2.5 mm, 30 cardiac phases

measured in a single plane, underestimating eccentric regurgitations. Newer 4-D velocity-encoded phase contrast acquisitions allow for more accurate quantification of flow and regurgitant volumes and are able to visualize 3-D flow patterns (Fig. 8) [52, 53]. Furthermore, 4-D velocity-encoded MR is a free-breathing technique and, using compressed sensing and parallel imaging, high spatial resolutions can be obtained (near isotropic 3 mm^3) [52, 53]. The high spatial resolutions even proved sufficient to accurately quantify ventricular volumes in the same 4-D dataset [19]. Furthermore, the desired slice orientation can be determined offline after acquisition. These advantages make 4-D phase contrast acquisitions very valuable in pediatric patients

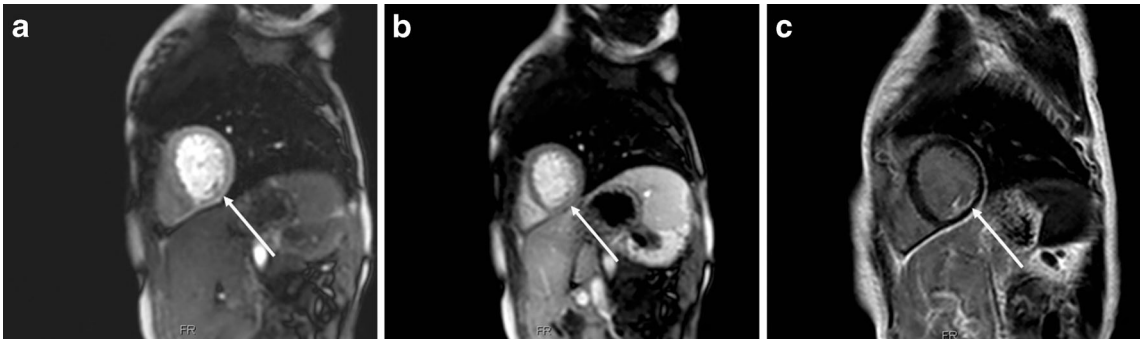

Fig. 7 Myocardial perfusion in a 19-year-old woman with an anomalous left circumflex coronary artery from the pulmonary artery, which was reimplanted in the aortic root at 13 years of age. A routine follow-up nuclear myocardial perfusion scan was inconclusive and an adenosine stress myocardial perfusion cardiac magnetic resonance imaging was performed. Stress perfusion images (**a**) show a subendocardial perfusion defect in the mid-inferior wall, which is not seen in the matching rest perfusion images (*arrows*) (**b**). The late gadolinium enhancement image (**c**) shows limited subendocardial hyperenhancement in the same area (*arrow*), suggesting a mid-inferior region with subendocardial ischemia and a limited irreversible component. For myocardial perfusion imaging, a single-shot balanced-fast field echo sequence with 100 ms saturate prepulse was performed directly after administering contrast both at rest and during adenosine stress. Images were taken in short axis (3 slices), 4-chamber and 2-chamber orientation with the following scan parameters: TR/TE 2.6/1.31 ms, flip angle 50°, matrix 128×141, voxel size 2.73×2.86 mm, slice thickness 10 mm (with a gap of 9.05 mm for short-axis slices) and 60 dynamic phases

with congenital heart diseases, in whom complex anatomy can make accurate slice orientation difficult. Disadvantages remain the relatively long acquisition times of 5–15 min and the longer postprocessing time.

Tissue characterization

Late gadolinium enhancement

Imaging of focal fibrosis using late gadolinium enhancement is incorporated into standard imaging protocols of both ischemic and nonischemic cardiomyopathies in many institutions. Currently, 2-D late gadolinium enhancement with (phase-sensitive) inversion-recovery (PSIR) gradient echo sequence still is the reference standard to assess viability of myocardium on cardiac MR imaging (Fig. 9) [54–56]. In pediatric patients, 2-D late gadolinium enhancement can be performed using respiratory gated free-breathing, achieving equal imaging quality as repeated breath-holds [57]. However, 3-D acquisition seems preferable as signal-to-noise ratio is improved for late gadolinium enhancement imaging, facilitating increased spatial resolution [58]. Without acceleration, 3-D imaging is time-consuming and artifacts may occur due to changes in inversion time and heart rate during the acquisition, both negatively influencing myocardial nulling. Compressed

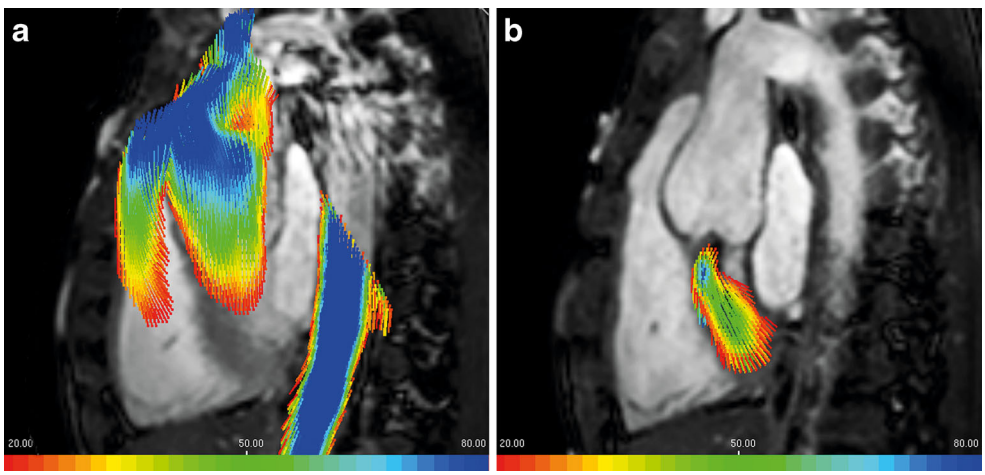

Fig. 8 Four-dimensional velocity-encoded imaging. Visualization of the systolic flow patterns in the left ventricular outflow tract and ascending aorta (**a**), and of neo-aortic valve regurgitation (**b**) in a 16-year-old boy after arterial switch operation for transposition of the great arteries. A color scale is used to visualize the flow velocities recorded using 4-D velocity-encoded imaging. Images were acquired using a 3-D gradient echo with Cartesian acquisition with the following scan parameters: TR/TE 7.7/4.2 ms, flip angle 10°, matrix 108×60, acquired voxel size 3.43×3.65×3.50 mm, 18 slices using 30 phases and three directions of flow encoding

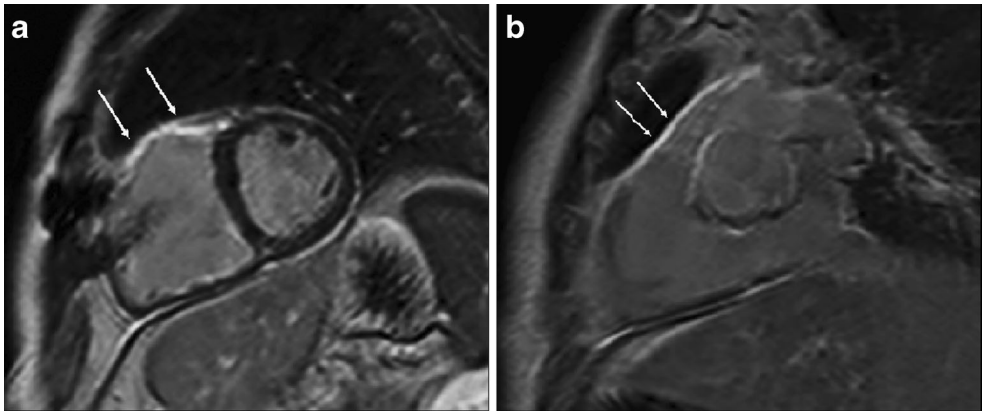

Fig. 9 Conventional late gadolinium enhancement imaging in a 45-year-old patient after repair for Tetralogy of Fallot with suspected cardiac sarcoidosis. Late gadolinium enhancement imaging was performed in short axis (**a**) and right ventricular outflow tract view (**b**) 15 min after administration of 0.2 mmol/kg gadolinium contrast agent. Delayed hyperenhancement can be seen at the sight of the homograft implantation (*arrows* in **a** and **b**). This is a typical finding in patients after homograft implantation and is not suspect for cardiac involvement of sarcoidosis. An inversion-recovery gradient echo was performed using the following imaging parameters: TR/TE 3.5/1.15 ms, flip angle25°, matrix 160×131, acquired voxel size 2x2.44x10 mm, 10 slices

sensing is one of the techniques proposed to facilitate 3-D late gadolinium enhancement imaging with high isotropic spatial resolution in short acquisition time (Fig. 10). The increased resolution is not only of importance for the pediatric population but was also shown to increase the success of radiofrequency ablation procedures in patients with recurrent ventricular arrhythmia. Adaptations to conventional compressed sensing have been proposed, such as low-dimensional-structure self-learning and thresholding, which reduces blurring artifacts and can achieve high isotropic resolution [59]. To prevent imperfect myocardial nulling due to changes in inversion time, PSIR can be used [55] or acquisition times can be shortened by improving the efficiency of respiratory gating with for example continuously adaptive windowing strategy [60].

Myocardial edema

Imaging of acute myocardial edema using cardiac magnetic resonance imaging was described as early as 1991 by Gagliardi et al. [9], demonstrating altered signal intensity using T2-weighted spin-echo sequences in the presence of myocarditis. Short-tau-inversion recovery (STIR) black-blood technique proved superior to T2-weighted spin-echo for musculoskeletal and abdominal MR and was introduced for cardiac imaging 1996 by Simonetta et al. [61]. They demonstrated that STIR can generate myocardial images which are highly sensitive to changes in tissue relaxation times, with minimum flow and motion artifacts (Fig. 11). Although introduced in the 1990s, it was not until 2004 that STIR was validated in a larger group of patients to establish its sensitivity to distinguish acute (myocardial edema) from chronic (fibrosis) myocardial infarction, with success [10]. The same research group tested the diagnostic value of a comprehensive cardiac MR imaging protocol to diagnose myocarditis, using presence of early relative enhancement (gRE), presence of late gadolinium enhancement and high signal intensity – relative to skeletal muscle – on T2-weighted black-blood STIR, as diagnostic criteria [62]. The

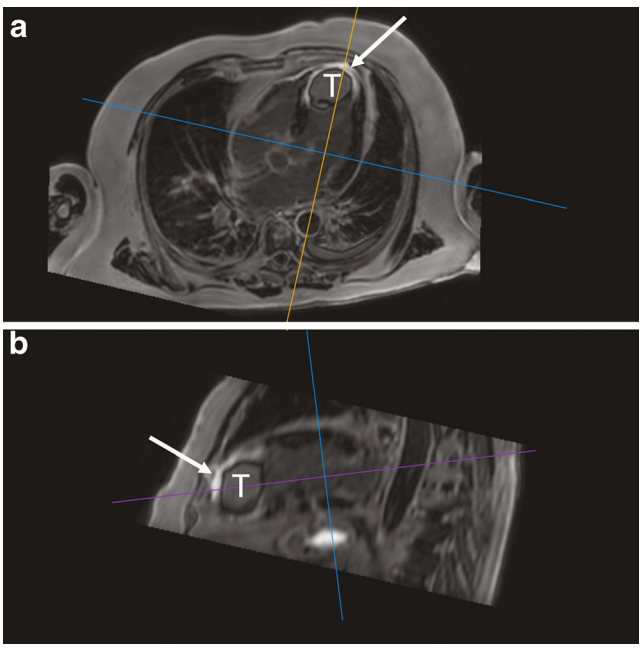

Fig. 10 Near-isotropic free-breathing 3-D late gadolinium enhancement sequence. Assessment of myocardial late gadolinium enhancement and presence of thrombus in a 50-year-old uncooperative male stroke patient with severe cardiac arrhythmia. Image acquisition was done during free-breathing and 3 signals averaged to reduce motion artifacts. A 3-D inversion-recovery gradient echo sequence was employed 15 min after administration of 0.2 mmol/kg gadolinium contrast agent. Imaging parameters used were: TR/TE 3.5/1.2 ms, flip angle 25°, matrix 93×87, acquired voxel size 3.43×3.65×5.00 mm, 32 slices. In the 4-chamber orientation (**a**), a large thrombus is present in the left ventricular apex (marked with T), surrounded by transmurally infarcted myocardium (*arrows*). Because of the nearly isotropic spatial resolution reformations in the left 2-chamber (**b**) and short-axis orientations could be made after completion of the acquisition

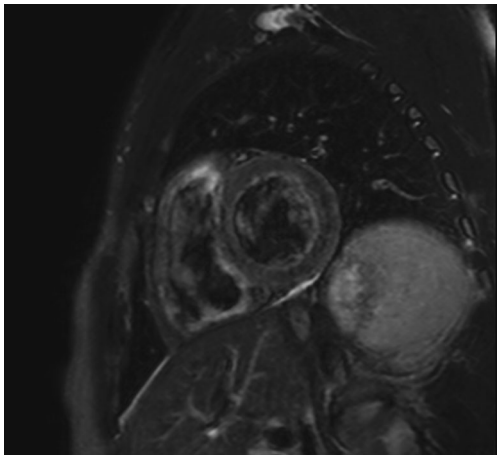

Fig. 11 Myocardial edema in myocarditis in a 22-year-old man with suspected perimyocarditis. A T2-weighted short-T1 inversion (STIR) recovery sequence in short-axis orientation reveals subtle diffusely increased signal of the myocardium, which is most clearly seen when myocardial signal intensity is compared to that of skeletal muscle in the same image. The diffusely increased signal intensity indicates that there is diffuse myocardial edema, which is in line with a diagnosis of myocarditis. The following scan parameters were used: TR/TE: 2,182/100 ms, flip angle 90°, matrix 236×175, acquired voxel size 1.36×1.83 mm, slice thickness 8 mm, 15 slices

highest diagnostic accuracy was achieved if all three were combined and ≥2 features were positive, which was later adapted to the Lake Louise consensus criteria for suspected myocarditis on cardiac MR imaging [63, 64]. However, black-blood STIR has some important limitations such as signal drop-out, slow-flow blood artifacts, image quality impairment in tachycardia (or normal high heart rate in children) and lower signal-to-noise ratio. To achieve optimal image contrast and quality STIR sequence, parameters should be chosen carefully with special regard for timing and design of the pulse sequence, quality of the TSE readout pulses, bandwidth and slice thickness. To improve the robustness and clinical applicability of edema imaging on cardiac MR imaging, noncontrast sequences have been developed over the past years. Aletras et al. [65] propose Acquisition for Cardiac Unified T2 Edema (ACUT2E), a combined TSE-SFFP approach to achieve optimal CNR, signal-to-noise ratio and image quality to depict acute myocardial infarction with a reduction of artifacts, although the absolute T2 values are systematically overestimated with this method [65]. Furthermore, non-contrast T1 mapping (also see below) was compared to both conventional black-blood STIR and ACUT2E TSE-SSFP and yielded a higher diagnostic accuracy to detect acute myocardial infarction, even though more regions were affected by artifacts. The higher diagnostic accuracy is likely the result of eliminating the need to compare myocardium to a remote reference region of interest, which is mandatory for both black-blood STIR and ACUT2E [66]. Other advantages of T1 mapping include that it is robust to tachycardia and breath-holds are considerably shorter, making it advantageous for children.

T1 mapping

After the success of late gadolinium enhancement for imaging of focal fibrosis, much attention was directed to noninvasive quantification of diffuse myocardial fibrosis in the past decade. This process is presumed to be accelerated in many congenital and non-congenital cardiac diseases [67]. Multiple cardiac MR imaging methodologies have been developed to quantify diffuse myocardial fibrosis, using T1 mapping with or without contrast administration. First, a new imaging sequence was developed by Messroghli and colleagues to overcome the limitations of the conventional look-locker approach, the modified look-locker inversion recovery (MOLLI), which was later modified into shortened-MOLLI, both facilitating high-resolution T1 maps of the human myocardium within a single breath-hold [68, 69]. The first clinically applicable cardiac MR imaging method was validated against myocardial biopsy in 2010 by Flett and colleagues [70], using equilibrium-contrast cardiac MR imaging with a standard MOLLI acquired before and after contrast equilibrium. The theory behind this method is that at contrast equilibrium, the extracellular gadolinium concentration is equal in blood and myocardium and the extracellular volume fraction of the myocardium can be determined, which correlates well to collagen volume fraction on biopsy. However, although accurate and highly repeatable, time to contrast equilibrium is relatively long and multiple breath-holds are required making this a complex and time-consuming technique, especially if used in children [70]. Several solutions were developed in the past years to shorten and simplify acquisition. First, to simplify the contrast protocol a bolus-only technique – assuming dynamic equilibrium – was designed. Both contrast protocols – bolus vs. continuous infusion – were compared to each other and to histological results by White and colleagues [71]. The bolus-only proved equally accurate in estimating extracellular volume fraction, provided the total fraction was less than 0.4 [71]. Extent of diffuse myocardial fibrosis, measured by bolus or equilibrium-contrast T1 mapping, has since been linked to decreased functional status and outcome in several pathologies, including congenital heart disease and childhood cancer survivors [72–74]. To further simplify the acquisition, a third contrast protocol was investigated by Miller and colleagues [75], using isolated postcontrast myocardial T1 measurement. In their study, isolated post bolus-contrast T1 measurement and extracellular volume fraction estimation using pre- and post-bolus-contrast T1 mapping was compared to histology, they conclude that isolated postcontrast T1 measurement is insufficient to reliably estimate extracellular volume fraction [75]. Finally, a protocol not requiring contrast administration, non-contrast

T1 mapping, was used to image diffuse myocardial fibrosis. It was compared to histology in patients with aortic stenosis and, although it only moderately correlated to collagen content measured on histology, T1 mapping was able to differentiate healthy from diseased and was related to the severity of aortic stenosis [76]. Following the rapid innovations in the area of quantification of extracellular volume fraction and T1 mapping, the cardiac MR imaging working group of the European Society of Cardiology and the Society of Cardiovascular Magnetic Resonance recently released a consensus statement. In accordance with the above stated, they observe that extracellular volume fraction measurement appears to be more accurate than isolated postcontrast T1 measurement (Fig. 12). Furthermore, they state that a bolus-only approach with at least 15-min delay is sufficient for most myocardial extracellular volume fraction applications.[77]

Imaging of stents and intracardiac devices

In patients with congenital heart disease, interventional devices and stents are increasingly used to decrease the need for surgery and increase convenience of the patient. Khan et al. [78] researched the disruption caused by the interventional devices and the influence of type of pulse sequence and field strength. Although signal void in the immediate vicinity of the device was common, significant disruption of surrounding tissue was only seen for the stainless steel Flipper detachable embolization coil. Field strength and pulse sequence type did not significantly influence image disruption or signal void [78]. Nordmeyer et al. [79] investigated the diagnostic accuracy of CT angiography and different cardiac magnetic resonance imaging sequences compared to conventional angiography to assess patency and re-stenosis of nitinol, platinum-iridium and stainless steel stents. Combining high flip angle gradient recalled echo, SSFP and high flip angle MRA resulted in high diagnostic accuracy for nitinol and platinum-iridium stents. For stainless steel stents the diagnostic accuracy compared to angiography was slightly lower due to large penumbra of signal loss [79].

Hybrid cardiac catheterizations, combining radiographic and MR imaging to accurately address clinical questions, are being performed for both diagnostic and interventional purposes. An obvious advantage of MR guiding is decreased radiation exposure, which predisposes to development of cancer, especially when radiation is imposed on smaller infants [80]. Other advantages include improved visualization of soft tissue and cardiac structures and the ability to combine invasive pressure measurements with flow quantification performed on cardiac MR imaging, ensuring accurate assessment of the hemodynamics and pulmonary vascular resistance [81]. The development of catheters is ongoing, currently passive guidewires – not actively conveying signals to the cardiac magnetic resonance imaging scanner – are used for such guided catheterizations, as active wires carry a risk of heating. Recently, a compatible and safe guidewire for MR imaging was developed and the first studies in children are currently being conducted [81].

Conclusion

Patients with congenital heart disease increasingly survive into adulthood and are in need of repeated high-quality cardiac MR imaging throughout life. The technical advances as outlined above enable high-fidelity assessment of anatomical as well as functional parameters and tissue characterization in short imaging times and underscore the preferential role of cardiac MR imaging as comprehensive cardiac imaging technique of first choice.

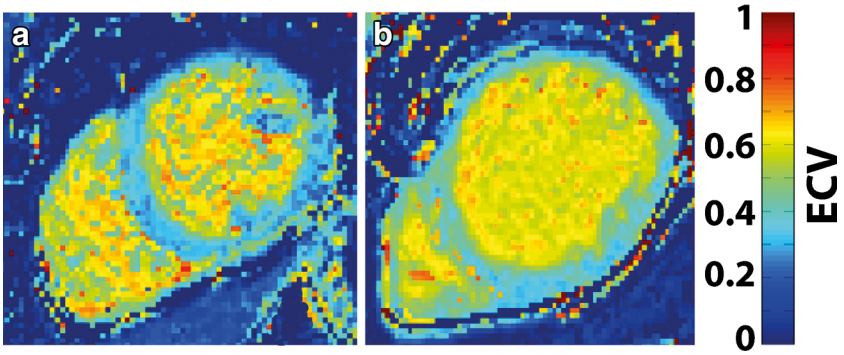

Fig. 12 T1 mapping and extracellular volume measurement. Examples illustrate extracellular volume maps in a patient with no abnormalities (a) and a patient with dilated cardiomyopathy (**b**). Note the larger extracellular volume fraction in the patient with dilated cardiomyopathy. Extracellular volume maps were obtained by acquiring two separate T1 maps with the modified look-locker 3–5 sequence: a single-shot balanced FFE readout (TR/TE 3.2/1.17 ms, flip angle 35°, matrix 288×288, acquired voxel 2×2×8 mm, 3 slices, SENSE=1.5). One map was obtained before contrast injection, and the second was acquired 15 min after bolus injection of 0.2 ml/kg contrast agent

Conflicts of interest None

References

1. Tennant PW, Pearce MS, Bythell M et al (2010) 20-year survival of children born with congenital anomalies: a population-based study. Lancet 375:649–656
2. van der Bom T, Bouma BJ, Meijboom FJ et al (2012) The prevalence of adult congenital heart disease, results from a systematic review and evidence based calculation. Am Heart J 164:568–575
3. Wren C, O'Sullivan JJ (2001) Survival with congenital heart disease and need for follow up in adult life. Heart 85:438–443
4. Towbin JA, Lowe AM, Colan SD et al (2006) Incidence, causes, and outcomes of dilated cardiomyopathy in children. JAMA 296:1867–1876
5. Nugent AW, Daubeney PE, Chondros P et al (2003) The epidemiology of childhood cardiomyopathy in Australia. N Engl J Med 348: 1639–1646
6. Lipshultz SE, Lipsitz SR, Sallan SE et al (2005) Chronic progressive cardiac dysfunction years after doxorubicin therapy for childhood acute lymphoblastic leukemia. J Clin Oncol 23:2629–2636
7. Hinton DP, Wald LL, Pitts J et al (2003) Comparison of cardiac MRI on 1.5 and 3.0 Tesla clinical whole body systems. Invest Radiol 38: 436–442
8. Dietrich O, Reiser MF, Schoenberg SO (2008) Artifacts in 3-T MRI: physical background and reduction strategies. Eur J Radiol 65:29–35
9. Gagliardi MG, Bevilacqua M, Di Renzi P et al (1991) Usefulness of magnetic resonance imaging for diagnosis of acute myocarditis in infants and children, and comparison with endomyocardial biopsy. Am J Cardiol 68:1089–1091
10. Abdel-Aty H, Zagrosek A, Schulz-Menger J et al (2004) Delayed enhancement and T2-weighted cardiovascular magnetic resonance imaging differentiate acute from chronic myocardial infarction. Circulation 109:2411–2416
11. Cohen MS, Weisskoff RM, Rzedzian RR et al (1990) Sensory stimulation by time-varying magnetic fields. Magn Reson Med 14:409–414
12. Budinger TF, Fischer H, Hentschel D et al (1991) Physiological effects of fast oscillating magnetic field gradients. J Comput Assist Tomogr 15:909–914
13. Pruessmann KP, Weiger M, Scheidegger MB et al (1999) SENSE: sensitivity encoding for fast MRI. Magn Reson Med 42:952–962
14. Sodickson DK, Manning WJ (1997) Simultaneous acquisition of spatial harmonics (SMASH): fast imaging with radiofrequency coil arrays. Magn Reson Med 38:591–603
15. Leiner T, Habets J, Versluis B et al (2013) Subtractionless first-pass single contrast medium dose peripheral MR angiography using two-point Dixon fat suppression. Eur Radiol 23:2228–2235
16. Tsao J, Kozerke S (2012) MRI temporal acceleration techniques. J Magn Reson Imaging 36:543–560
17. Lustig M, Donoho D, Pauly JM (2007) Sparse MRI: The application of compressed sensing for rapid MR imaging. Magn Reson Med 58: 1182–1195
18. Vasanawala SS, Chan FP, Newman B et al (2011) Combined respiratory and cardiac triggering improves blood pool contrast-enhanced pediatric cardiovascular MRI. Pediatr Radiol 41:1536–1544
19. Hsiao A, Lustig M, Alley MT et al (2012) Rapid pediatric cardiac assessment of flow and ventricular volume with compressed sensing parallel imaging volumetric cine phase-contrast MRI. AJR Am J Roentgenol 198:W250–259
20. Stuber M, Botnar RM, Danias PG et al (1999) Double-oblique free-breathing high resolution three-dimensional coronary magnetic resonance angiography. J Am Coll Cardiol 34:524–531
21. Lai P, Larson AC, Park J et al (2008) Respiratory self-gated four-dimensional coronary MR angiography: a feasibility study. Magn Reson Med 59:1378–1385
22. Stehning C, Bornert P, Nehrke K et al (2005) Free-breathing whole-heart coronary MRA with 3D radial SSFP and self-navigated image reconstruction. Magn Reson Med 54:476–480
23. Spincemaille P, Nguyen TD, Prince MR et al (2008) Kalman filtering for real-time navigator processing. Magn Reson Med 60:158–168
24. van Heeswijk RB, Bonanno G, Coppo S et al (2012) Motion compensation strategies in magnetic resonance imaging. Crit Rev Biomed Eng 40:99–119
25. Vignaux OB, Augui J, Coste J et al (2001) Comparison of single-shot fast spin-echo and conventional spin-echo sequences for MR imaging of the heart: initial experience. Radiology 219: 545–550
26. Karaus A, Merboldt KD, Graessner J et al (2007) Black-blood imaging of the human heart using rapid stimulated echo acquisition mode (STEAM) MRI. J Magn Reson Imaging 26:1666–1671
27. Hernandez RJ, Strouse PJ, Londy FJ et al (2001) Gadolinium-enhanced MR angiography (Gd-MRA) of thoracic vasculature in an animal model using double-dose gadolinium and quiet breathing. Pediatr Radiol 31:589–593
28. Vogt FM, Theysohn JM, Michna D et al (2013) Contrast-enhanced time-resolved 4D MRA of congenital heart and vessel anomalies: image quality and diagnostic value compared with 3D MRA. Eur Radiol 23:2392–2404
29. Young PM, McGee KP, Pieper MS et al (2013) Tips and tricks for MR angiography of pediatric and adult congenital cardiovascular diseases. AJR Am J Roentgenol 200:980–988
30. Fenchel M, Saleh R, Dinh H et al (2007) Juvenile and adult congenital heart disease: time-resolved 3D contrast-enhanced MR angiography. Radiology 244:399–410
31. Dabir D, Naehle CP, Clauberg R et al (2012) High-resolution motion compensated MRA in patients with congenital heart disease using extracellular contrast agent at 3 Tesla. J Cardiovasc Magn Reson 14: 75
32. Naehle CP, Kaestner M, Muller A et al (2010) First-pass and steady-state MR angiography of thoracic vasculature in children and adolescents. JACC Cardiovasc Imaging 3:504–513
33. Yoon YE, Kitagawa K, Kato S et al (2012) Prognostic value of coronary magnetic resonance angiography for prediction of cardiac events in patients with suspected coronary artery disease. J Am Coll Cardiol 60:2316–2322
34. Kato S, Kitagawa K, Ishida N et al (2010) Assessment of coronary artery disease using magnetic resonance coronary angiography: a national multicenter trial. J Am Coll Cardiol 56:983–991
35. Greenwood JP, Maredia N, Radjenovic A et al (2009) Clinical evaluation of magnetic resonance imaging in coronary heart disease: the CE-MARC study. Trials 10:62
36. Bornert P, Koken P, Nehrke K et al (2013) Water/fat-resolved whole-heart Dixon coronary MRA: An initial comparison. Magn Reson Med 54:476–480
37. Leiner T, Katsimaglis G, Yeh EN et al (2005) Correction for heart rate variability improves coronary magnetic resonance angiography. J Magn Reson Imaging 22:577–582
38. Jaroni J, Meier R, Beer A et al (2013) Three-dimensional magnetic resonance imaging using single breath-hold k-t BLAST for assessment of global left ventricular functional parameters. Acad Radiol 20: 987–994
39. Parish V, Hussain T, Beerbaum P et al (2010) Single breath-hold assessment of ventricular volumes using 32-channel coil technology and an extracellular contrast agent. J Magn Reson Imaging 31:838–844
40. Stralen van M, Habets J, Driessen M et al. (2012) Dual breath-hold 3D whole heart cine cardiac MRI: feasibility and initial experience [abstract 3843]. ISMRM
41. Makowski MR, Wiethoff AJ, Jansen CH et al (2012) Single breath-hold assessment of cardiac function using an accelerated 3D single breath-hold acquisition technique–comparison of

an intravascular and extravascular contrast agent. J Cardiovasc Magn Reson 14:53
42. Bellenger NG, Gatehouse PD, Rajappan K et al (2000) Left ventricular quantification in heart failure by cardiovascular MR using prospective respiratory navigator gating: comparison with breath-hold acquisition. J Magn Reson Imaging 11: 411–417
43. Coelho-Filho OR, Rickers C, Kwong RY et al (2013) MR myocardial perfusion imaging. Radiology 266:701–715
44. Ebersberger U, Makowski MR, Schoepf UJ et al (2013) Magnetic resonance myocardial perfusion imaging at 3.0 Tesla for the identification of myocardial ischaemia: comparison with coronary catheter angiography and fractional flow reserve measurements. Eur Heart J Cardiovasc Imaging 14:1174–1180
45. Watkins S, McGeoch R, Lyne J et al (2009) Validation of magnetic resonance myocardial perfusion imaging with fractional flow reserve for the detection of significant coronary heart disease. Circulation 120:2207–2213
46. Cheng AS, Pegg TJ, Karamitsos TD et al (2007) Cardiovascular magnetic resonance perfusion imaging at 3-tesla for the detection of coronary artery disease: a comparison with 1.5-tesla. J Am Coll Cardiol 49:2440–2449
47. Manso B, Castellote A, Dos L et al (2010) Myocardial perfusion magnetic resonance imaging for detecting coronary function anomalies in asymptomatic paediatric patients with a previous arterial switch operation for the transposition of great arteries. Cardiol Young 20:410–417
48. Prakash A, Powell AJ, Krishnamurthy R et al (2004) Magnetic resonance imaging evaluation of myocardial perfusion and viability in congenital and acquired pediatric heart disease. Am J Cardiol 93: 657–661
49. Dulce MC, Mostbeck GH, O'Sullivan M et al (1992) Severity of aortic regurgitation: interstudy reproducibility of measurements with velocity-encoded cine MR imaging. Radiology 185:235–240
50. Brenner LD, Caputo GR, Mostbeck G et al (1992) Quantification of left to right atrial shunts with velocity-encoded cine nuclear magnetic resonance imaging. J Am Coll Cardiol 20:1246–1250
51. Fujita N, Chazouilleres AF, Hartiala JJ et al (1994) Quantification of mitral regurgitation by velocity-encoded cine nuclear magnetic resonance imaging. J Am Coll Cardiol 23: 951–958
52. Westenberg JJ, Roes SD, Ajmone Marsan N et al (2008) Mitral valve and tricuspid valve blood flow: accurate quantification with 3D velocity-encoded MR imaging with retrospective valve tracking. Radiology 249:792–800
53. Hsiao A, Lustig M, Alley MT et al (2012) Evaluation of valvular insufficiency and shunts with parallel-imaging compressed-sensing 4D phase-contrast MR imaging with stereoscopic 3D velocity-fusion volume-rendered visualization. Radiology 265: 87–95
54. Kim RJ, Fieno DS, Parrish TB et al (1999) Relationship of MRI delayed contrast enhancement to irreversible injury, infarct age, and contractile function. Circulation 100:1992–2002
55. Kellman P, Arai AE, McVeigh ER et al (2002) Phase-sensitive inversion recovery for detecting myocardial infarction using gadolinium-delayed hyperenhancement. Magn Reson Med 47:372–383
56. Kim RJ, Wu E, Rafael A et al (2000) The use of contrast-enhanced magnetic resonance imaging to identify reversible myocardial dysfunction. N Engl J Med 343:1445–1453
57. Goldfarb JW, Shinnar M (2006) Free-breathing delayed hyperenhanced imaging of the myocardium: a clinical application of real-time navigator echo imaging. J Magn Reson Imaging 24:66–71
58. Peters DC, Appelbaum EA, Nezafat R et al (2009) Left ventricular infarct size, peri-infarct zone, and papillary scar measurements: A comparison of high-resolution 3D and conventional 2D late gadolinium enhancement cardiac MR. J Magn Reson Imaging 30:794–800
59. Akcakaya M, Rayatzadeh H, Basha TA et al (2012) Accelerated late gadolinium enhancement cardiac MR imaging with isotropic spatial resolution using compressed sensing: initial experience. Radiology 264:691–699
60. Keegan J, Jhooti P, Babu-Narayan SV et al (2013) Improved respiratory efficiency of 3D late gadolinium enhancement imaging using the continuously adaptive windowing strategy (CLAWS). Magn Reson Med. doi:10.1002/mrm.24758
61. Simonetti OP, Finn JP, White RD et al (1996) "Black blood" T2-weighted inversion-recovery MR imaging of the heart. Radiology 199:49–57
62. Abdel-Aty H, Boye P, Zagrosek A et al (2005) Diagnostic performance of cardiovascular magnetic resonance in patients with suspected acute myocarditis: comparison of different approaches. J Am Coll Cardiol 45:1815–1822
63. Friedrich MG, Sechtem U, Schulz-Menger J et al (2009) Cardiovascular magnetic resonance in myocarditis: A JACC White Paper. J Am Coll Cardiol 53:1475–1487
64. Chu GC, Flewitt JA, Mikami Y et al (2013) Assessment of acute myocarditis by cardiovascular MR: diagnostic performance of shortened protocols. Int J Cardiovasc Imaging 29: 1077–1083
65. Aletras AH, Kellman P, Derbyshire JA et al (2008) ACUT2E TSE-SSFP: a hybrid method for T2-weighted imaging of edema in the heart. Magn Reson Med 59:229–235
66. Ferreira VM, Piechnik SK, Dall'Armellina E et al (2012) Non-contrast T1-mapping detects acute myocardial edema with high diagnostic accuracy: a comparison to T2-weighted cardiovascular magnetic resonance. J Cardiovasc Magn Reson 14:42
67. Dweck MR, Joshi S, Murigu T et al (2011) Midwall fibrosis is an independent predictor of mortality in patients with aortic stenosis. J Am Coll Cardiol 58:1271–1279
68. Messroghli DR, Radjenovic A, Kozerke S et al (2004) Modified look-locker inversion recovery (MOLLI) for high-resolution T1 mapping of the heart. Magn Reson Med 52: 141–146
69. Fontana M, White SK, Banypersad SM et al (2012) Comparison of T1 mapping techniques for ECV quantification. Histological validation and reproducibility of ShMOLLI versus multibreath-hold T1 quantification equilibrium contrast CMR. J Cardiovasc Magn Reson 14:88
70. Flett AS, Hayward MP, Ashworth MT et al (2010) Equilibrium contrast cardiovascular magnetic resonance for the measurement of diffuse myocardial fibrosis: preliminary validation in humans. Circulation 122:138–144
71. White SK, Sado DM, Fontana M et al (2013) T1 mapping for myocardial extracellular volume measurement by CMR: bolus only versus primed infusion technique. JACC Cardiovasc Imaging 6:955–962
72. Plymen CM, Sado DM, Taylor AM et al (2013) Diffuse myocardial fibrosis in the systemic right ventricle of patients late after Mustard or Senning surgery: an equilibrium contrast cardiovascular magnetic resonance study. Eur Heart J Cardiovasc Imaging 14:963–968
73. Tham EB, Haykowsky MJ, Chow K et al (2013) Diffuse myocardial fibrosis by T1-mapping in children with

subclinical anthracycline cardiotoxicity: relationship to exercise capacity, cumulative dose and remodeling. J Cardiovasc Magn Reson 15:48
74. Wong TC, Piehler K, Meier CG et al (2012) Association between extracellular matrix expansion quantified by cardiovascular magnetic resonance and short-term mortality. Circulation 126:1206–1216
75. Miller CA, Naish JH, Bishop P et al (2013) Comprehensive validation of cardiovascular magnetic resonance techniques for the assessment of myocardial extracellular volume. Circ Cardiovasc Imaging 6: 373–383
76. Bull S, White SK, Piechnik SK et al (2013) Human non-contrast T1 values and correlation with histology in diffuse fibrosis. Heart 99: 932–937
77. Moon JC, Messroghli DR, Kellman P et al (2013) Myocardial T1 mapping and extracellular volume quantification: a Society for Cardiovascular Magnetic Resonance (SCMR) and CMR Working Group of the European Society of Cardiology consensus statement. J Cardiovasc Magn Reson 15:92
78. Khan SN, Rapacchi S, Levi DS et al (2013) Pediatric cardiovascular interventional devices: effect on CMR images at 1.5 and 3 Tesla. J Cardiovasc Magn Reson 15:54
79. Nordmeyer J, Gaudin R, Tann OR et al (2010) MRI may be sufficient for noninvasive assessment of great vessel stents: an in vitro comparison of MRI, CT, and conventional angiography. AJR Am J Roentgenol 195:865–871
80. Andreassi MG (2009) Radiation risk from pediatric cardiac catheterization: friendly fire on children with congenital heart disease. Circulation 120:1847–1849
81. Tzifa A, Schaeffter T, Razavi R (2012) MR imaging-guided cardiovascular interventions in young children. Magn Reson Imaging Clin N Am 20:117–128